

# Femtosecond laser-induced microstructures on Ti substrates for reduced cell adhesion

J. Heitz<sup>1</sup>  · C. Plamadala<sup>1</sup> · M. Muck<sup>1</sup> · O. Armbruster<sup>1</sup> · W. Baumgartner<sup>2</sup> · A. Weth<sup>2</sup> · C. Steinwender<sup>3</sup> · H. Blessberger<sup>3</sup> · J. Kellermair<sup>3</sup> · S. V. Kirner<sup>4</sup> · J. Krüger<sup>4</sup> · J. Bonse<sup>4</sup> · A. S. Guntner<sup>5</sup> · A. W. Hassel<sup>5</sup>

Received: 2 September 2017 / Accepted: 27 October 2017  
© The Author(s) 2017. This article is an open access publication

**Abstract** Miniaturized pacemakers with a surface consisting of a Ti alloy may have to be removed after several years from their implantation site in the heart and shall, therefore, not be completely overgrown by cells or tissue. A method to avoid this may be to create at the surface by laser-ablation self-organized sharp conical spikes, which provide too little surface for cells (i.e., fibroblasts) to grow on. For this purpose, Ti-alloy substrates were irradiated in the air by 790 nm Ti:sapphire femtosecond laser pulses at fluences above the ablation threshold. The laser irradiation resulted in pronounced microstructure formation with hierarchical surface morphologies. Murine fibroblasts were seeded onto the laser-patterned surface and the coverage by cells was evaluated after 3–21 days of cultivation by means of scanning electron microscopy. Compared to flat surfaces, the cell density on the microstructures was significantly lower, the coverage was incomplete, and the cells had a clearly different morphology. The best results regarding suppression of cell growth were obtained on spike structures which were additionally electrochemically oxidized under acidic conditions.

Cell cultivation with additional shear stress could reduce further the number of adherent cells.

## 1 Introduction

New miniaturized and smart medical devices are more and more used in all medical fields, including miniaturized pacemakers. Via a catheter, these miniaturized pacemakers are directly implanted into the right ventricle of the heart [1]. The pacemakers with a surface consisting of a Ti alloy may have to be removed after several years (for instance, at the end of the battery lifetime of the device) and shall, therefore, not be completely overgrown by the cells or scar tissue after implantation [2]. Cardiovascular implants consisting, for instance, of Ti or Ti alloys often have surfaces which are repellent for adsorption of proteins and cells to avoid clotting or stenosis. This is achieved by surface modification or coating with thin films [3–5]. The aim of these treatments is either to make the surface bioinert, to apply coatings which release pharmaceutical drugs or agents preventing adsorption of cells or proteins, or to make the surface bioactive that it can be covered by endothelial cells which form the natural linings of the blood vessels. The surface modifications are also done to suppress corrosion and fouling of the implants in the human body environment and, for applications in hard tissues, to reduce friction and wear or to increase the osteointegration [6–8].

Laser structuring offers a simple contactless one-step process for controlling the surface morphology of almost arbitrary materials ranging from transparent organic polymers to strongly absorbing metals [9]. Even when the irradiation is performed with a homogeneous spatial laser beam profile, repeated irradiation of the same surface spot by several laser pulses transforms the roughened surfaces via inter-pulse

✉ J. Heitz  
johannes.heitz@jku.at

<sup>1</sup> Institute of Applied Physics, Johannes Kepler University Linz, Altenberger Straße 69, 4040 Linz, Austria

<sup>2</sup> Institute of Biomedical Mechatronics, Johannes Kepler University Linz, Altenberger Straße 69, 4040 Linz, Austria

<sup>3</sup> Department of Cardiology, Kepler University Hospital Linz, Krankenhausstraße 9, 4020 Linz, Austria

<sup>4</sup> Bundesanstalt für Materialforschung und -prüfung (BAM), Unter den Eichen 87, 12205 Berlin, Germany

<sup>5</sup> Christian Doppler Laboratory for Combinatorial Oxide Chemistry (at Institute for Chemical Technology of Inorganic Materials), Johannes Kepler University Linz, Altenberger Straße 69, 4040 Linz, Austria

feedback phenomena into characteristic self-ordered surface morphologies, such as nanometric laser-induced periodic surface structures (LIPSS) [10–13] or micrometer-sized grooves and conical spikes [14, 15]. The feedback mechanism during repetitive treatments selects specific spatial periods of the roughness distribution that can absorb radiation better [16]. If laser scan processing with Gaussian beams is employed for structuring of large surface areas, the latter micrometer-sized spike structures are usually covered by the sub-micrometric LIPSS structures, resulting in hierarchical surface morphologies. The latter surfaces are often strongly hydrophobic, featuring the well-known water repellent *Lotus effect* [17]. The amount of different self-ordered surface structures renders various ways of particular surface functionalization possible—as demonstrated in applications for surface colorization [18], the reduction of friction and wear [19], the control of cell or biofilm growths [20, 21], or the promotion of protein adsorption [22].

Ranella et al. [23] have demonstrated that femtosecond laser-induced conical spikes on silicon surfaces can hinder the adhesion of fibroblast cells, at least for several days in culture. The laser irradiation was performed in an SF<sub>6</sub> atmosphere and the resulting surface with the laser-induced microstructures was super-hydrophobic. The suppression of the cell adhesion was probably due to the fact that the microstructures are too dense and sharp for the cells to fill the gaps in between the spikes and that the resulting surface for cell adhesion at the structure tips becomes just too small to form enough adhesion junctions in the cell membrane. In addition, the chemical composition of the surface is important. When the surface was oxidized, it became not only super-hydrophilic, but it also could be colonized by the fibroblast cells. The confinement of the area of adhesion has also been reported for other laser-induced structures. We showed, for instance, in an earlier publication that shallow laser-induced LIPSS structures on polymers with a period of 250–300 nm restricted the cell-surface contact to the structure tops, while the cells could follow laser-induced structures with a wider periodicity [24]. These findings are in good agreement with the recent work of Yiannakou et al. [25] on femtosecond laser-induced structures on Si irradiated in water. They showed that LIPSS structures on Si with a periodicity of about 150 nm suppressed cell adhesion, while coarser (but not too sharp) laser-induced structures in the  $\mu\text{m}$  range could be well colonized by cells.

Titanium is like aluminum, niobium, tantalum, and others a valve metal, which forms in contact with the air or aqueous solutions at its surface a stable passive oxide film. The native thin-oxide layer can be thickened upon anodic polarization [26, 27], which, for Ti, is accompanied by a visible color change [6, 28]. This electrochemical oxide growth occurs via high-field-assisted migration of Ti cations outwards and of oxygen ions inwards. Local oxidation was performed by

means of a flow-type scanning droplet cell microscope (FT-SDCM) for which the measuring head was manufactured by 3D printing [29]. The thickness, composition, crystallinity, and charge distribution of the Ti–O films influence strongly their interaction with cells and other biological materials. For instance, it has been shown that oxide layers formed by ion implantation, sputtering, or ion beam enhanced deposition provided a good hemocompatibility of Ti surfaces [30, 31]. Proteins adsorbed on an oxidized Ti substrate prior to its colonization by cells had a major influence on initiating and directing cellular activities. It has been shown that Ti–O surfaces with sponge-like texture formed by chemical oxidation of Ti films with H<sub>2</sub>SO<sub>4</sub>/H<sub>2</sub>O<sub>2</sub> could significantly promote or limit the adhesion of specific proteins [32].

In the current work, we investigate whether it is possible to suppress cell adhesion on a Ti-alloy surface (with a similar composition as that of the casings of the miniaturized heart pacemakers) by laser-induced nano- or microstructures in combination with electrochemical surface oxidation. For the cell tests, we chose murine fibroblasts. The cell cultivation was done either under static conditions or with additional shear stress mimicking the blood stream.

## 2 Experimental

### 2.1 Ti-alloy substrates

Commercial grade-5 Ti-alloy samples (Ti6Al4V, 3.7165) were purchased from Schumacher Titan GmbH (Solingen, Germany) as rods of 25 mm diameter. These rods were cut into circular slabs of 8 mm thickness and were mechanically polished, resulting in a mirror-like surface finish with an average roughness  $R_a < 10$  nm. For control experiments, 1 mm-thick flat medical grade Ti6Al4V samples with an area of  $20 \times 20$  mm<sup>2</sup> were employed, which were purchased from Zapp Precision Metals GmbH (Schwerte, Germany).

### 2.2 Laser-induced microstructure formation on Ti substrates

For laser processing, a Ti:sapphire femtosecond laser amplifier system (Femtolasers, Compact Pro) was used, generating linearly polarized laser pulses ( $\tau = 30$  fs,  $\lambda = 790$  nm center wavelength,  $f = 1$  kHz pulse repetition frequency). The laser pulse energies  $E$  were measured by means of a pyroelectric detector (Coherent 3 $\Sigma$ , J-25LP-3A-2K head). The laser pulses were focused by a spherical dielectric mirror of 500 mm focal length.

The samples were mounted on a motorized  $x$ – $y$ – $z$  linear translation stage (Micos VT-80, Germany) and placed normal to the incident laser beam. In the geometrical laser focus, a Gaussian-like spatial beam profile with a radius  $w_0$

$(1/e^2) < 29\text{--}73\ \mu\text{m}$  was measured. The corresponding peak fluence,  $\phi_0$ , in front of the sample surface was calculated via  $\phi_0 = 2E/(\pi w_0^2)$ . By line-wise meandering movement of the sample under the focused laser beam (scan velocity  $v_x = 0.145\text{--}0.365\ \text{mm/s}$ , line-offset  $\Delta y = 0.015\text{--}0.05\ \text{mm}$ ), areas from  $2 \times 2$  to  $8 \times 8\ \text{mm}^2$  were processed. At these conditions, the effective number of laser pulses per focused laser spot diameter  $D = 2w_0$  (for a single laser-processing pass) accounted to  $N_{\text{eff}} = (D \times f)/v_x$  [33] in the scan direction. These processing parameters corresponded to a laser peak fluence of  $\phi_0 \sim 3.0\ \text{J/cm}^2$  along with an effective number of laser pulses of  $N_{\text{eff}} \sim 400$ . Using an ultrasonic bath, the samples were cleaned in acetone after the laser processing.

The morphology of the laser-processed surfaces was characterized by scanning electron microscopy (SEM, Carl Zeiss Gemini Supra 40).

### 2.3 Contact angle measurements

To evaluate and compare the wetting properties of the unprocessed Ti-alloy surfaces with the laser-irradiated and chemically treated surfaces, contact angle measurements were performed. Prior to the measurements, the sample was rinsed with ethanol to remove possible impurities and dried. The sessile drop method was used to measure the static contact angle on the different surfaces. Each time, a droplet of  $1\ \mu\text{l}$  of distilled water was used. For each surface, five contact angle measurements were performed and the mean values and standard deviations were calculated.

### 2.4 Coverage by murine fibroblasts

#### 2.4.1 Cells and cell culture

Cells from a murine fibroblast cell line, namely, LTK (ECACC 85011432, UK), were used as test system. They were grown in DMEM (Lactan, Graz, Austria) + 2 mM Glutamine (Sigma) + 10% Foetal Calf Serum (FCS, Biochrom, Berlin, Germany), supplemented with 50 U/ml Penicillin + Streptomycin (Serva, Heidelberg, Germany) in  $\text{H}_2\text{O}$ -saturated atmosphere with 5%  $\text{CO}_2$  at  $37\ ^\circ\text{C}$ . They were split typically once a week at a ratio of 1:10. Finally, the cells were seeded onto the Ti-alloy samples with the laser-written microstructures, which were placed in Petri dishes, and cultivated as described above for 3–21 days.

For shear stress experiments, a home built cone rheometer with a tip angle of  $5^\circ$  was used. Revolution speed was adjusted yielding a shear stress of  $1\ \text{dyn/cm}^2$ . Cells were sheared in the incubator for 5 days.

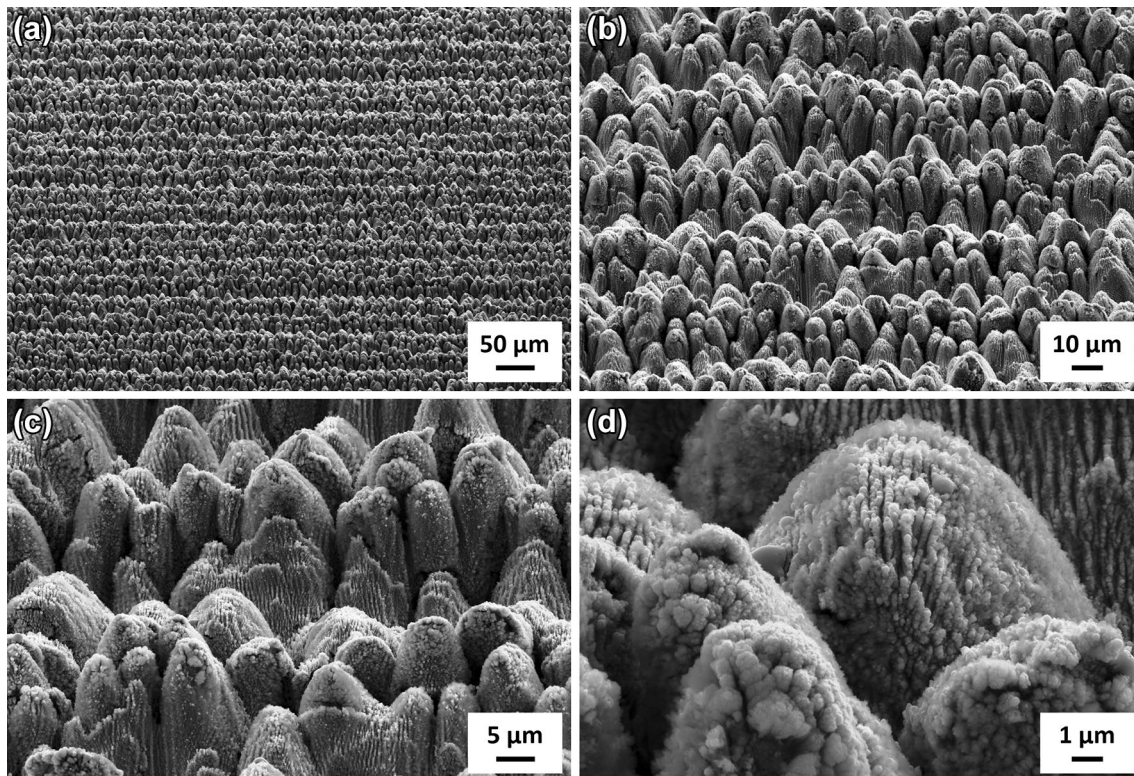
#### 2.4.2 Electron microscopy of cell covered surfaces

Cell attachment at the surface and cell morphology was evaluated by means of scanning electron microscopy (SEM). For this, the cells were fixed with 6% glutaraldehyde (GA; Merck, Darmstadt, Germany) in PBS (phosphate buffered saline) over night followed by dehydration by means of ascending ethanol series (30, 40, 50, 70, 80, 90, 96%,  $3 \times 100\%$ ) 30 min each. Then, the samples were transferred into 100% hexamethyl-disilazane (HMDS; Merck). HMDS was exchanged three times. The HMDS was evaporated over night. Finally, samples were sputter-coated with gold. SEM images were obtained with a Philips SEM 525 (Philips, Germany) at 15 kV.

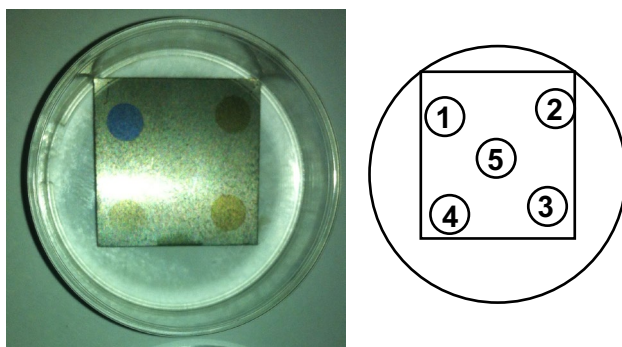
## 3 Results

Figure 1 shows SEM images of laser-induced microstructures on a Ti-alloy surface after irradiation with about 400 fs Ti:sapphire laser pulses per spot at a fluence above the ablation threshold, taken at four different magnifications. The images were acquired under a tilt angle of  $60^\circ$ . The surface is covered by quasi-periodic conical spikes with a spacing of about  $5\ \mu\text{m}$  and a height of  $> 5\ \mu\text{m}$ . Due to the line-wise scanning of the laser spot, the spikes are arranged in rows, which is most obvious in Fig. 1a. The spike structures are covered by more regular parallel sub-micrometric LIPSS grating structures, resulting in a hierarchical surface morphology. The periodicity of the LIPSS grating is about 300–350 nm, which is considerably lower than the laser wavelength of  $\lambda = 790\ \text{nm}$ . The linear polarization of the laser beam is parallel to the grating vector of the LIPSS structures.

Figure 2a shows a Ti-alloy sample after electrochemical oxidation at five spots with a diameter of about 3.5 mm. The spot 5 in the middle is hardly visible. The sample is covered by cells and is, therefore, placed in a Petri dish. The arrangement of the five spots is schematically shown in Fig. 2b. The electrochemical treatment of the different spots is described in Table 1. The oxidized spots have a gold, brown, or blue color, which correspond according to reference [6] to an oxide layer thickness of about 10, 25, or 40 nm, respectively. However, it is not clear whether those results can be directly transferred to our investigations, as it is, for instance, not clear which specific Ti-alloy composition and treatment conditions were used there. However, it is consistent that the spot 1 with the highest applied voltage (potentiostatic, 18 V) and the longest treatment time is blue and that spots 2 and 3 with potentiodynamic 0–10 V have a darker gold/brown hue than spots 4 and 5 with potentiodynamic 0–3 V. Under the same conditions, the spots treated in NaOH were darker than those treated in  $\text{H}_2\text{SO}_4$ .



**Fig. 1** SEM images (60° tilted view) of spikes on Ti-alloy surface induced by irradiation with about 400 fs Ti:sapphire laser pulses per spot (wavelength  $\lambda = 790$  nm, linear polarization)



**Fig. 2** Photograph of 20×20 mm<sup>2</sup> Ti-alloy sample with five electrochemically oxidized spots (schematically shown at the right). The chemical treatments are listed in Table 1

SEM images of fibroblasts 2 weeks after seeding are shown in Fig. 3. On a flat Ti-alloy substrate without laser processing or electrochemical treatment (Fig. 3a), the cells are confluent and form dense multi-layers. The cells have an elongated shape (which is typical for fibroblasts), but show no preferred orientation over longer distances. Fibroblasts grown on areas with laser-induced conical spikes (Fig. 3b) are separated and seem to grow only on the tips of the spikes. Between the cells, there are free spaces, where the underlying laser-patterned Ti-alloy surface is visible. While it was easy to distinguish in the SEM laser-treated areas covered by cells from flat untreated areas covered by cells, the distinction between electrochemically treated areas covered by cells and flat untreated areas covered by cells was difficult, at least

**Table 1** Electrochemical-processing conditions and water contact angles of the five differently chemically treated spots at the Ti-alloy surface

Spot	1	2	3	4	5
Electrochemical processing	18 V, 1000 s, 0.1 mol NaOH	0–10 V, 100 mV/s, 0.1 mol NaOH	0–10 V, 100 mV/s, 0.1 mol H <sub>2</sub> SO <sub>4</sub>	0–3 V, 1 mV/s, 0.1 mol NaOH	0–3 V, 1 mV/s, 0.1 mol H <sub>2</sub> SO <sub>4</sub>
Contact angle	58° ± 10°	71° ± 4°	62° ± 11°	62° ± 9°	61° ± 9°

Spot 1 was treated potentiostatically, spots 2–5 potentiodynamically (potentials measured versus standard hydrogen electrode SHE)

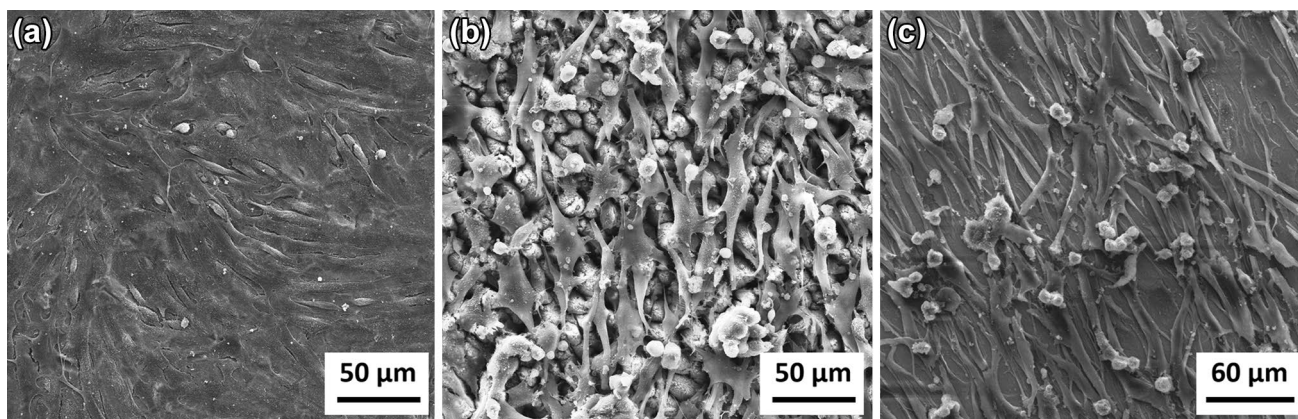
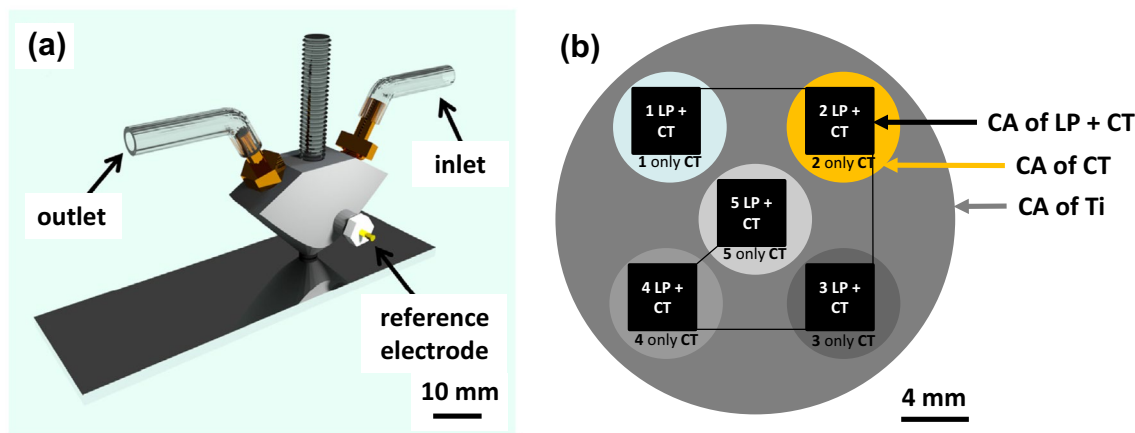


**Fig. 3** SEM images of fibroblasts 2 weeks after seeding on **a** flat Ti-alloy substrate, **b** Ti-alloy substrate with Ti:sapphire laser-induced spikes (as shown in Fig. 1), and **c** electrochemically oxidized Ti-alloy substrate (under condition as spot 5 in Table 1)

in the SEM images. We had to mark the visible colored spots with scratches. A closer look, however, showed that the cells on the electrochemically treated areas (for example, in Fig. 3c) have a more pronounced shape than those on the untreated areas (Fig. 3a), which may be an indication that their density is lower. The fact that there are more spherical small cells, which are not adherent and are not integrated into the cell layers is, however, not systematic. Such cells are also visible on other places at untreated areas (not shown) and on the laser-processed area, as shown in Fig. 3b. Here, they are hard to distinguish in the SEM image from the spikes.

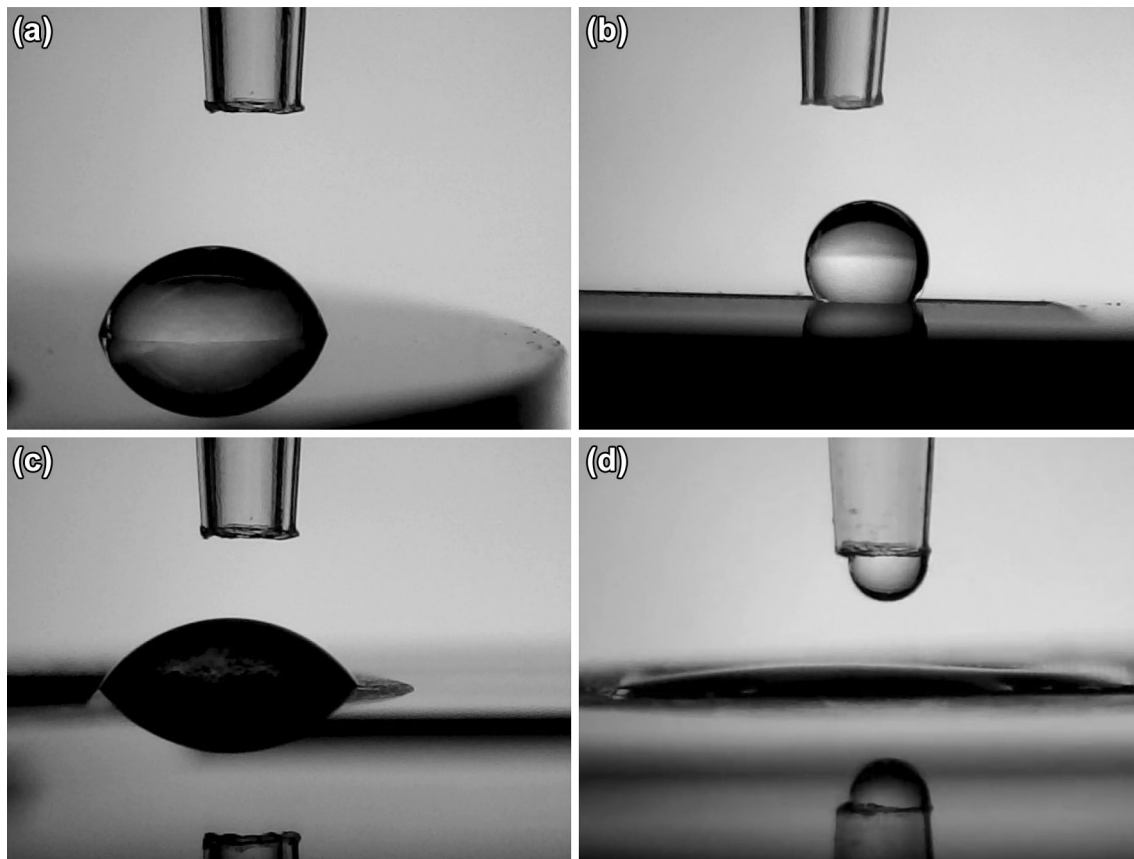
Figure 4a shows the schematics of the head of the FT-SDCM setup used for the electrochemical treatment. The orifice of the head had a diameter of 7 mm, which was chosen to overlap the full 4 × 4 mm<sup>2</sup> areas of the laser processing. The arrangement of the different areas is shown in

Fig. 4b. The round spots (1–5) are the five electrochemically treated spots (with the conditions in Table 1) and the black rectangles were laser processed before the chemical treatment. The black lines between the rectangles indicate the fact that the laser was not switched off when moving from one rectangle to another. The sample was large enough that water contact angle (CA) measurements could be performed on areas which were laser processed and chemically treated (LP + CT), only chemically treated (CT), or unprocessed (Ti). The contact angle value on the unprocessed Ti-alloy area (shown in grey in Fig. 4b) is about  $75^\circ \pm 5^\circ$ , i.e., it is moderately hydrophilic (Fig. 5a). The contact angle on the laser structured area (with no additional treatment) has a value of  $113^\circ \pm 10^\circ$ , that is, laser irradiation renders the Ti-alloy surface hydrophobic (Fig. 5b). The contact angle values for the five chemically treated Ti-alloy surfaces are summarized in Table 1. It can be seen that the chemical treatment



**Fig. 4** Graphical sketch of **a** flow-type scanning droplet cell microscope setup and **b** Ti-alloy sample showing unprocessed surface in grey, five differently chemically treated areas (1–5, as shown in

Table 1) in different hues, and the laser-processed areas, which were subsequently chemically treated, in black



**Fig. 5** Side view of droplets of distilled water on **a** untreated Ti-alloy sample; **b** laser-processed Ti-alloy sample without chemical treatment; **c** Ti-alloy surface with chemical treatment of spot 1 in Table 1

without laser processing; and **d** laser-processed Ti alloy with chemical treatment of spot 1 in Table 1

made the Ti-alloy surface more hydrophilic (Fig. 5c). The contact angle measurements on the laser processed and later chemically treated areas showed that a combination of these two factors (surface roughness and chemistry) resulted in an even more hydrophilic surface. When applying a droplet of water, it immediately spread on the surface, forming a contact angle lower than  $15^\circ$  (Fig. 5d).

An SEM image of the rim between a laser-processed area with spikes and flat Ti surface is shown in Fig. 6a. Both areas were also electrochemically oxidized under acidic conditions (the same as spot 3 in Table 1). Clearly visible are the laser-induced microstructures at the right side of the image. Figure 6b shows the same sample at a similar position after cultivation with fibroblasts for 1 week. While on the only chemically treated flat area, the fibroblast form multi-layers with additional spherical non-adherent cells, which sometimes form clusters, only few adherent cells can be found on the right side of the image of Fig. 6b. The sample had again five spots with different electrochemical treatment conditions (i.e., those of Table 1). Regarding suppression of cell adhesion, the best result was obtained for the conditions of spot 3 in Table 1, the second best for the conditions of spot

5. For both spots, the electrochemical oxidation was performed in  $\text{H}_2\text{SO}_4$  (with two different potentiodynamic voltage ranges and different scan rates). Another sample, again with five spots treated under the conditions of Table 1, was kept for 2 weeks in the cell culture and then evaluated. The results remained qualitatively the same (e.g., best suppression of cell adhesion for spot 3), even though more cells were found on the laser-processed areas. On the upper right side of Fig. 6b, there are a few adherent spread fibroblasts at the laser-processed area and also spherical small non-adherent cells. It seems that the latter are also present in the lower right side of the image, but it is again difficult to distinguish them in the SEM image from the spikes.

The suppression of the cell adhesion can be increased if the cell culture is not performed under static conditions but with additional shear stress. This is shown in Fig. 7 for a sample which was kept for 5 days in culture with a shear stress of  $1 \text{ dyn/cm}^2$ , which is produced by a rotating cone in the culture dish. Again, the best result regarding suppression of cell adhesion was obtained for the conditions of spot 3 in Table 1, which is also shown in the figure. There are no adherent cells in the laser-processed

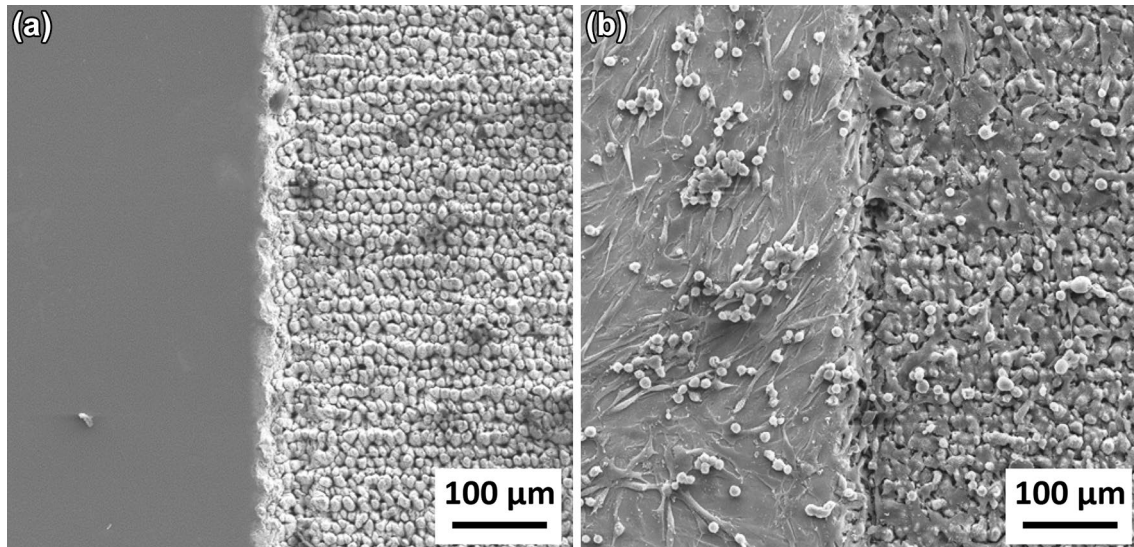


**Fig. 6** SEM images of rim between flat untreated Ti-alloy surface and Ti-alloy surface with Ti:sapphire laser-induced spikes combined with electrochemical oxidation: **a** without cells and **b** with fibroblasts 1 week after seeding

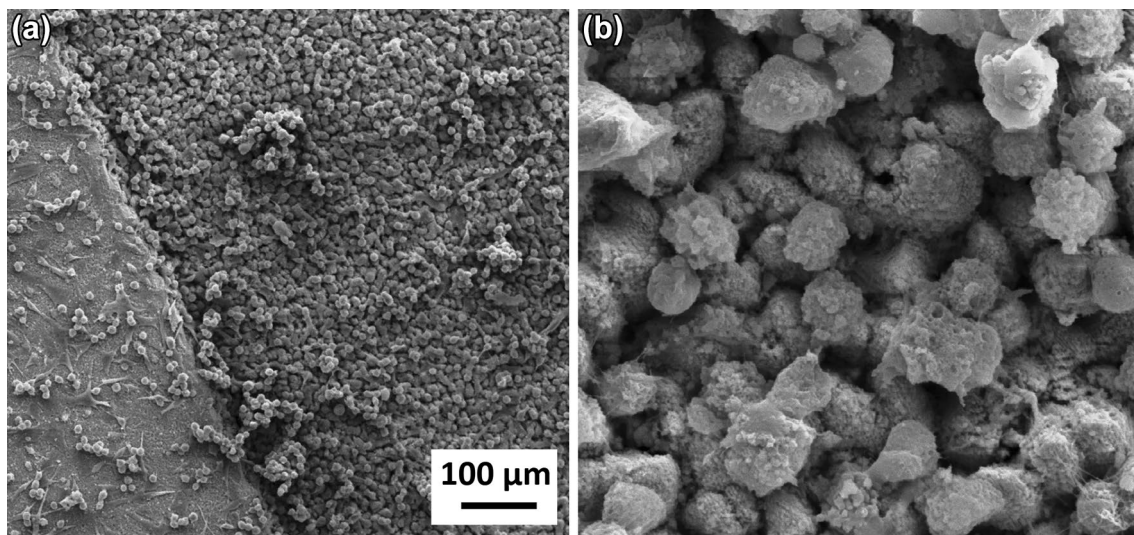


**Fig. 7** SEM images of results from shear stress experiments: **a** rim between flat Ti-alloy surface and Ti-alloy surface with Ti:sapphire laser-induced spikes, both areas combined with electrochemical oxidation

(under condition as spot 3 in Table 1); **b** magnification in the area of laser-induced spikes

area, but only spherical non-adherent cells, which sometimes form clusters. Most of the laser-processed area is completely free of cells. LIPSS sub-structures on the spikes are visible in many places of the magnified image, as shown in Fig. 7b. On the lower right edge of Fig. 7b, a closer look also reveals some fibrillar material which is most probably collagen produced by the fibroblasts, as this is typical for this cell type.

#### 4 Discussion

The thermal penetration depth  $l_{th}$  for laser processing is given by  $l_{th} = (D \times \tau)^{1/2}$ , where  $\tau$  is the laser pulse length and  $D$  is the thermal diffusivity [9]. In control experiments, we irradiated the Ti-alloy surfaces with  $\lambda = 284$  nm KrF excimer laser pulses with pulse lengths of  $\tau = 20$  ns and a fluence above the ablation threshold and observed only surface

melting without formation of conical spikes, probably due to the larger value of  $l_{th}$  compared to femtosecond laser treatment. Just on the rim of the irradiated spots, we found sharp features (with dimensions similar to the spikes in Fig. 1), which were probably formed by re-solidified melt splashes. We seeded cells on these features and found some influence on the cell morphology and cell density, but much less pronounced than for the femtosecond laser-induced spikes, as shown in Fig. 3b. These nanosecond laser-induced microstructures were also smooth and not covered by finer LIPSS patterns, as the process for their formation is mostly thermal and the laser radiation also was not linearly polarized. Therefore, the worse results regarding suppression of cell adhesion may also be attributed to the missing LIPSS structure.

The features of the structured and oxidized Ti-alloy surface address three different aspects in cell adhesion. The flexibility of an adherent mammalian cell is limited, and therefore, it cannot follow sharp surface features like the laser-induced spikes. The contact area is limited to the tips of the spikes, which considerably weakens the possible adhesion forces. The trans-membrane adhesion proteins in the cell membrane (i.e., the integrins) are clustered to focal adhesions which have sub- $\mu\text{m}$  lateral dimensions and typical distances of up to a few  $\mu\text{m}$ . The effect of sub- $\mu\text{m}$  LIPSS structures is probably that they restrict the number of focal adhesions which are in contact with the ridges of the ripples leading also to weaker adsorption. In addition, forced unfavorable distances of the focal adhesions in the cell membrane may induce cell-internal signal pathways leading to a separation from the surface. It is assumed that the individual integrins are not connected directly to the surface of an implant or cell-culture substrate but to extra-cellular matrix proteins, which are adsorbed on the surface, either originating from the surrounding medium or produced by the cell itself. The oxidation of the surface may additionally limit the adhesion of important adhesion-promoting proteins or promote the adhesion of adhesion-limiting proteins (as suggested in [32] for various proteins) if the properties of the oxide layer are optimized for this purpose.

As we have shown in Fig. 5d, the areas with laser-induced spikes and additional electrochemical oxidation are highly hydrophilic. This is remarkable as many (but not all) bioinert surfaces, like Teflon, are hydrophobic, which may cause problems regarding clotting in contact to blood. We also tested blood and other body fluids and found that the surfaces of Fig. 5d are completely wettable by these fluids. This seems to be in accordance with the findings in the references [30, 31], which claim that oxidized Ti surfaces are hemocompatible.

We performed our cell test with fibroblasts and not with endothelial cells, which form the natural inner linings of blood vessels, because the histological analysis of the tissue around an encapsulated pacemaker in reference [2] revealed

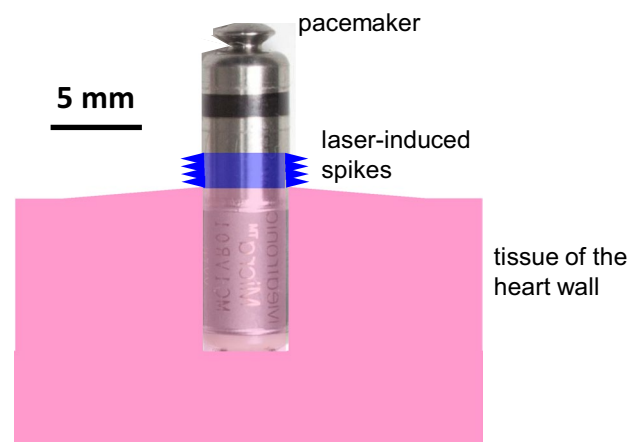


**Fig. 8** Schematics of envisaged ingrowth of miniaturized pacemaker with laser-induced spikes

that it consisted mainly of scar tissue, i.e., of fibroblasts and extra-cellular matrix proteins like collagen produced by these cells. Murine fibroblasts from cell lines are renowned for their excellent adhesion properties. Thus, it can be expected that a surface which is repellent for these cells also repels primary adherent cells of this and other cell types.

The shear stress experiments reported here were performed at a rather low shear stress rate of  $1 \text{ dyn/cm}^2$  compared to  $5 \text{ dyn/cm}^2$ , which is a typical value for the venous system. We expect that in vivo, in the body blood stream, non-adherent cells and also extra-cellular matrix material would be washed away even more efficiently than in our in vitro experiments at low shear rates, where we already see clear effects.

For the application with the implantable miniaturized pacemakers, one would probably only pattern a relatively narrow ring around the casing of the pacemaker with laser-induced spikes. As it is shown schematically in Fig. 8a, this ring should control the depth of the ingrowth of the implant into the heart wall. Probably, one would arrange the rows of the spikes around the casing perpendicular to the axis.

## 5 Conclusions

The Ti-alloy TiAl6V4 is often used for medical implants. We showed that femtosecond laser irradiation of that material can result in the formation of sharp conical spikes which are covered by sub-wavelength laser-induced periodic surface structures. We could demonstrate for the first time that in combination with electrochemical oxidation, these structures form a cell-repellent surface which is also hydrophilic. These surfaces may have interesting applications in the field of medical implants or prostheses, which have to be removed

from the body some time after the implantation or which should be overgrown only partially.

**Acknowledgements** Open access funding provided by Johannes Kepler University Linz. This work was supported by the Austrian Research Promotion Agency FFG under Grant No. 853390 (“LaMi-CellPro”) and the EU Horizon 2020 FETOPEN programme by project “LiNaBioFluid” (Grant Agreement No. 665337). Financial support by the Austrian Ministry of Economy, Family and Youth and the National Foundation for Research, Technology and Development is also gratefully acknowledged (Christian Doppler Laboratory for Combinatorial Oxide Chemistry). The authors would like to thank S. Benemann (BAM 6.1) and H. Habibzadeh (JKU IAP) for SEM characterization and S. Binkowski (BAM 6.3) for polishing the titanium samples. We also want to thank D. Bäuerle for initiating this cooperation and Medtronic Österreich GmbH for the interest in our investigations.

**Open Access** This article is distributed under the terms of the Creative Commons Attribution 4.0 International License (<http://creativecommons.org/licenses/by/4.0/>), which permits unrestricted use, distribution, and reproduction in any medium, provided you give appropriate credit to the original author(s) and the source, provide a link to the Creative Commons license, and indicate if changes were made.

## References

1. C. Steinwender, S. Hönig, K. Saleh, J. Kammler, H. Blessberger, S. Schwarz, A. Nahler, V. Gammer, M. Grund, A. Kypta, Wien. Klin. Wochenschr. **126**, S78 (2014)
2. A. Kypta, H. Blessberger, J. Kammler, M. Lichtenauer, T. Lambert, R. Silye, C. Steinwender, Can. J. Cardiol. **32**, 1578.e1 (2016)
3. P. Qi, M.F. Maitz, N. Huang, Surf. Coat. Technol. **233**, 80 (2013)
4. M.T. Mohammed, Z.A. Khan, A.N. Siddiquee, Proc. Mater. Sci. **6**, 1610 (2014)
5. X. Liu, P.K. Chu, C. Ding, Mater. Sci. Eng. R **47**, 49 (2004)
6. A.D. Revathi, A.I. Borras, C. Munoz, G. Richard, Manivasagam, Mater. Sci. Eng. C **76**, 1354 (2017)
7. K. Cai, Y. Hu, K.D. Jandt, Y. Wang, J. Mater. Sci. Mater. Med. **19**, 499 (2008)
8. C. Blaszykowski, S. Sheikh, M. Thompson, Chem. Soc. Rev. **41**, 5599 (2012)
9. D. Bäuerle, *Laser Processing and Chemistry*, 4th edn. (Springer, Berlin, 2011)
10. H.M. van Driel, J.E. Sipe, J.F. Young, Phys. Rev. Lett. **49**, 1955 (1982)
11. A.E. Siegman, P.M. Fauchet, IEEE J. Quantum Electron. **22**, 1384–1403 (1986)
12. A.Y. Vorobyev, C. Guo, Laser Photon. Rev. **7**, 385 (2013)
13. J. Bonse, S. Höhm, S.V. Kirner, A. Rosenfeld, J. Krüger, IEEE J. Sel. Top. Quantum Electron. **23**, 9000615 (2017)
14. J. Heitz, J.D. Pedarnig, D. Bäuerle, G. Petzow, Appl. Phys. A **65**, 259–261 (1997)
15. A.K.M. Tanvir, C. Grambow, A.M. Kietzig, Micromachines **5**, 1219–1253 (2014)
16. M. Abere, M. Zhong, J. Krüger, J. Bonse, MRS Bull. **41**, 969 (2016)
17. F. Müller, C. Kunz, S. Gräf, Materials **9**, 476 (2016)
18. B. Dusser, Z. Sagan, H. Soder, N. Faure, J.P. Colombier, M. Jourlin, E. Audouard, Opt. Express **18**, 2913 (2010)
19. J. Bonse, R. Koter, M. Hartelt, D. Spaltmann, S. Pentzien, S. Höhm, A. Rosenfeld, J. Krüger, Appl. Phys. A **117**, 103 (2014)
20. E. Rebollar, I. Frischauf, M. Olbrich, T. Peterbauer, S. Hering, J. Preiner, P. Hinterdorfer, C. Romanin, J. Heitz, Biomaterials **29**, 1796 (2008)
21. N. Epperlein, F. Menzel, K. Schwibbert, R. Koter, J. Bonse, J. Sameith, J. Krüger, J. Toepel, Appl. Surf. Sci. **418**, 420 (2017)
22. D. Kuczynska, P. Kwasniak, J. Marczak, J. Bonarski, J. Smolik, H. Garbacz, Appl. Surf. Sci. **390**, 560 (2016)
23. M. Ranella, S. Barberoglou, C. Bakogianni, E. Fotakis, Stratakis, Acta Biomater. **6**, 2711 (2010)
24. M. Schernthaner, G. Leitinger, H. Wolinski, S.D. Kohlwein, B. Reisinger, R.A. Barb, W.F. Graier, J. Heitz, K. Groschner, J. Nanomater. **2013**, 251063 (2013)
25. C. Yiannakou, C. Simitzi, A. Manousaki, C. Fotakis, A. Ranella, E. Stratakis, Biofabrication **9**, 025024 (2017)
26. J.P. Kollender, A.I. Mardare, A.W. Hassel, Electrochem. Commun. **74**, 5 (2017)
27. A.I. Mardare, C.D. Grill, I. Pötzelberger, T. Etzelstorfer, J. Stangl, A.W. Hassel, J. Solid State Electrochem. **20**, 1673 (2016)
28. S. Van Gils, P. Mast, E. Stijns, H. Terryn, Surf. Coat. Technol. **185**, 303 (2004)
29. J.P. Kollender, M. Voith, S. Schneiderbauer, A.I. Mardare, A.W. Hassel, J. Electroanal. Chem. **740**, 53 (2015)
30. N. Huang, P. Yang, Y.X. Leng, J.Y. Chen, H. Sun, J. Wang, G.J. Wang, P.D. Ding, T.F. Xi, Y. Leng, Biomaterials **24**, 2177 (2003)
31. N. Huang, P. Yang, X. Cheng, Y. Leng, X. Zheng, G. Cai, Z. Zhen, F. Zhang, Y. Chen, X. Liu, T. Xi, Biomaterials **19**, 771 (1998)
32. L. Richert, F. Variola, F. Rosei, J.D. Wuest, A. Nanci, Surf. Sci. **604**, 1445 (2010)
33. J. Bonse, G. Mann, J. Krüger, M. Marcinkowski, M. Eberstein, Thin Solid Films **542**, 420 (2013)